Local condensation of charge-4e superconductivity at a nematic domain wall

Matthias Hecker and Rafael M. Fernandes
School of Physics and Astronomy, University of Minnesota, Minneapolis, Minnesota 55455, USA

(Received 8 November 2023; revised 12 March 2024; accepted 3 April 2024; published 24 April 2024)

In the fluctuation regime that precedes the onset of pairing in multicomponent superconductors, such as nematic and chiral superconductors, the normal state is generally unstable toward the formation of charge-4e order—an exotic quantum state in which electrons form coherent quartets rather than Cooper pairs. However, charge-4e order is often suppressed by other competing composite orders, such as nematics. Importantly, the formation of nematic domains is unavoidable due to the long-range strains generated, leading to one-dimensional regions where the competing nematic order is suppressed. Here, we employ a real-space variational approach to demonstrate that, in such nematic domain walls, charge-4e order is locally condensed via a vestigial-order mechanism. We explore the experimental manifestations of this effect and discuss materials in which it can be potentially observed.

DOI: 10.1103/PhysRevB.109.134514

I. INTRODUCTION

Shortly after the development of the BCS model for superconductivity, it was recognized that a gas of bosons could also form a coherent state of pairs of bosons before the Bose-Einstein condensation of individual particles, provided that strong enough attractive interactions are present [1,2]. In nuclear matter, this concept has been employed to investigate the interplay between α-particle condensation and deuteron condensation [3]. In condensed matter systems, pair condensation of bosonic quasiparticles has been studied in various settings, from biexcitons in semiconductors [4,5] to two-magnon bound states in frustrated magnets [6,7]. A fascinating possibility is the emergence, in superconducting materials, of a coherent state of pairs of Cooper pairs, dubbed quartets [8–13]. Theoretically, while a microscopic description of charge-4e order remains elusive, a charge-4e superconducting state is expected to display gapless excitations [14,15] and half flux-quantum vortices [11]. Experimentally, the search for signatures of charge-4e superconductivity are ongoing. Recently, such a state has been invoked to explain puzzling magnetotransport data in kagome superconductors [16,17].

In the case of bosonic particles, the state with paired bosons is thermodynamically stable only when there is more than one bosonic "flavor" available for condensation (e.g., spin-1 bosons) [18,19]. This suggests that "multiflavor" superconductors are a promising setting to search for charge-4e superconductivity. Indeed, theoretical proposals for quartet formation have included multicondensate systems [20], spin-3/2 systems [21], spinor condensates [22], multiband superconductors [23], pair-density waves [11,24–30], and multicomponent superconductors [31–36]. In the latter case, the superconductor is described by multiple gap functions related by lattice symmetries, $\mathbf{\Delta} = (\Delta_1, \Delta_2, \cdots)$; in group-theory jargon, $\mathbf{\Delta}$ transforms as a multidimensional irreducible representation (IR) of the point group. There is a broad range of pairing states that belong to this category, including several versions of p-wave and d-wave states in tetragonal, hexagonal, and cubic lattices [37,38]. More importantly, there is experimental evidence for the realization of multicomponent pairing in various systems of interest, from heavy fermions [39–41] to moiré superlattices [42] to doped topological insulators [43–45].

The mechanism by which charge-4e order can emerge in multicomponent superconductors is via the condensation of a complex-valued composite order parameter, $\langle \mathbf{\Delta} \cdot \mathbf{\Delta} \rangle \neq 0$, while the superconducting order parameter itself remains zero, $\langle \mathbf{\Delta} \rangle = 0$ (the former is not to be confused with the real-valued composite $\langle \mathbf{\Delta}^\dagger \cdot \mathbf{\Delta} \rangle$, which is always nonzero as it breaks no symmetry) [31,46]. In other words, the transition temperature of the composite order, T_{4e}, must be larger than the superconducting transition temperature T_c. This spontaneous symmetry-breaking, which is driven by fluctuations and thus not captured by mean-field approaches, lowers the $U(1)$ gauge symmetry to Z_2; the latter is further broken if $\langle \mathbf{\Delta} \rangle$ becomes nonzero. It is said then that the charge-4e and charge-2e superconducting states are intertwined, and that the former is a vestigial order of the latter [47,48].

The main obstacle for the stabilization of charge-4e vestigial order is the competition with other vestigial phases, most notably nematic and ferromagnetic. Indeed, besides $U(1)$ symmetry, the ground state of a multicomponent superconductor also breaks either time-reversal (chiral superconductor) or rotational symmetry (nematic superconductor) [49]. These additional symmetries can be broken before the onset of superconductivity via the condensation of real-valued composite order parameters of the type $\langle \mathbf{\Delta}^\dagger \cdot \mathbf{\Lambda} \cdot \mathbf{\Delta} \rangle$, where $\mathbf{\Lambda}$ is a matrix in the subspace spanned by the components of $\mathbf{\Delta}$. Large-N and variational calculations found that the corresponding vestigial nematic and ferromagnetic orders generally preempt the onset of charge-4e order [50,51]—except for the special case of a hexagonal nematic superconductor [31].

In this work, we investigate whether the local suppression of the leading nematic or ferromagnetic vestigial order enables the local condensation of charge-4e order. While it is relatively well established that a subleading competing order

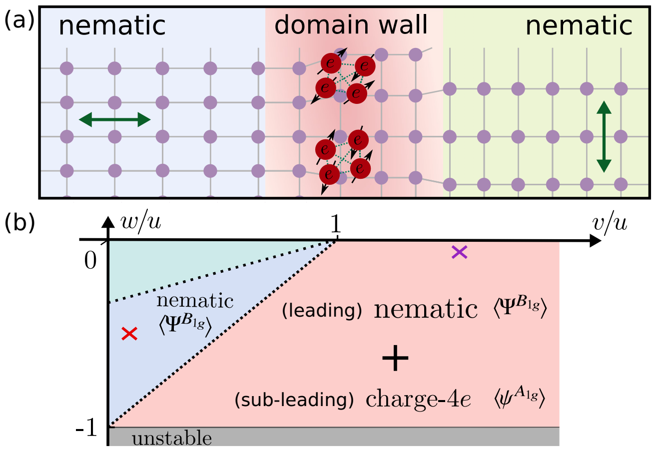

FIG. 1. (a) Real-space sketch of our main result, the emergence of charge-4e order at a nematic domain wall. (b) Phase diagram of the vestigial orders supported by the nematic superconducting ground state of a tetragonal system. Here, u, v, and w are the Landau parameters of Eq. (9). The different shaded regions indicate which vestigial channel is attractive: none (green), nematic (blue), and leading nematic with subleading charge-4e (red).

can condense when the leading order is locally suppressed [52], the situation we study in this paper is qualitatively different. Rather than two competing primary orders that break different symmetries and that must be tuned close to a multicritical point, here the two instabilities are both described by composite order parameters from the same primary superconducting order parameter, making them inevitably intertwined via the vestigial order mechanism [47,48].

We start in Sec. II by discussing a 2D triplet superconductor without spin-orbit coupling (SOC), whose multicomponent gap function has a continuous $SU(2)$ symmetry. In this case, the continuous symmetry globally forbids quasi-long-range order of any composite order parameter, except for charge-4e. Importantly, the vestigial phases emerging in this case are representative of the four types of vestigial phase found in other multicomponent superconductors, namely, ferromagnetic, nematic, s wave charge-4e, and d-wave charge-4e.

We then study the more realistic situation of discrete multicomponent superconductors in tetragonal and hexagonal systems in Sec. III. In this scenario, while long-range order in the competing vestigial channel is unavoidable, it is locally suppressed due to the formation of domains. Focusing on a nematic superconductor on the tetragonal lattice, we employ a real-space variational approach that treats all composite orders on an equal footing. We find a wide range of parameters for which charge-4e order is condensed at the nematic domain walls. Importantly, while superconducting fluctuations are enhanced near the domain walls, the superconducting order parameter remains uncondensed, resulting in a local charge-4e order, as illustrated schematically in Fig. 1(a). We finish in Sec. IV by discussing the qualitative experimental manifestations of this local condensation and candidate materials where this phenomenon may be realized. In Appendices A and B we provide details on the free energy derivation, and the implemented minimization strategy, respectively.

II. GLOBAL SUPPRESSION OF THE COMPETING VESTIGIAL PHASES

To set the stage, we discuss a special case in which, for symmetry reasons alone, the only order that can be stabilized is charge-4e. Consider a 2D system in which the electrons experience negligible SOC (e.g., graphene) and, in addition to spin, have another pseudospin degree of freedom (e.g., sublattice or valley). Enforcing the pairing state to be momentum independent and pseudospin singlet, the gap function must be spin triplet and represented by an order parameter $\boldsymbol{\Delta} = (\Delta_1,\ \Delta_2,\ \Delta_3)^T$ that transforms as a vector in $SU(2)$ spin space. This is nothing but the $\boldsymbol{d}$ vector of a triplet superconductor [37,38], albeit even in momentum. While there is no indication of valley-singlet spin-triplet superconductivity in graphene, this type of state has been studied in twisted moiré systems [53–56] and Bernal bilayer graphene [35,57]. The superconducting action is given by

$$\mathcal{S} = \int_{\mathsf{q}} \chi_{\mathsf{q}}^{-1} |\boldsymbol{\Delta}_{\mathsf{q}}|^2 + \int_{\mathsf{x}} (u|\boldsymbol{\Delta}_{\mathsf{x}}|^4 + v|\boldsymbol{\Delta}_{\mathsf{x}} \cdot \boldsymbol{\Delta}_{\mathsf{x}}|^2), \tag{1}$$

with (bare) superconducting susceptibility χ_{q}^{-1} and $\mathsf{q} = (\mathbf{q}, \omega_n)$ denoting momentum and Matsubara frequency. The interaction part has Landau coefficients u and v, where $\mathsf{x} = (\mathbf{x}, \tau)$ denotes position and imaginary time. The mean-field phase diagram of this model is well established [58,59], displaying different types of unitary and nonunitary pairing depending on the sign of v.

To describe the vestigial orders, however, it is necessary to go beyond mean field [48]; for our purposes, a group-theoretical analysis is sufficient. There are four symmetry-breaking bilinear combinations of $\boldsymbol{\Delta}$: two real-valued composites

$$\boldsymbol{\Psi}^{(l=1)} = \mathrm{i}\boldsymbol{\Delta} \times \bar{\boldsymbol{\Delta}}, \tag{2}$$

$$\Psi_{\mu\nu}^{(l=2)} = \frac{1}{2}(\Delta_\mu \bar{\Delta}_\nu + \Delta_\nu \bar{\Delta}_\mu) - \frac{1}{3}\,\delta_{\mu\nu}|\boldsymbol{\Delta}|^2, \tag{3}$$

and two complex-valued ones

$$\psi^{(l=0)} = \boldsymbol{\Delta} \cdot \boldsymbol{\Delta}, \tag{4}$$

$$\psi_{\mu\nu}^{(l=2)} = \Delta_\mu \Delta_\nu - \frac{1}{3}\,\delta_{\mu\nu}(\boldsymbol{\Delta} \cdot \boldsymbol{\Delta}), \tag{5}$$

where $\bar{z} \equiv z^*$. The superscript indicates the transformation properties in $SU(2)$ spin space, corresponding to a scalar ($l = 0$), a vector ($l = 1$), or a tensor ($l = 2$). Each composite has a clear physical interpretation: $\boldsymbol{\Psi}^{(l=1)}$ corresponds to time-reversal symmetry breaking and, thus, vestigial ferromagnetic order. $\Psi_{\mu\nu}^{(l=2)}$ is associated with rotational symmetry breaking in spin space, and therefore denotes (spin-)nematic vestigial order [34,60,61]. Finally, $\psi^{(l=0)}$ and $\psi_{\mu\nu}^{(l=2)}$ correspond to s-wave and d-wave charge-4e vestigial orders, respectively.

Because $\boldsymbol{\Psi}^{(l=1)}$, $\Psi_{\mu\nu}^{(l=2)}$, $\psi_{\mu\nu}^{(l=2)}$, and $\boldsymbol{\Delta} \equiv \boldsymbol{\Delta}^{(l=1)}$ itself transform nontrivially in $SU(2)$ spin space (i.e., they are at least Heisenberg-type order parameters), none of them can sustain (quasi-)long-range order at nonzero temperatures in 2D. On the other hand, because $\psi^{(l=0)}$ is a complex scalar (i.e., XY-type), it can establish quasi-long-range order through a BKT transition. Therefore, the only state allowed to develop quasi-long-range order in this model is the vestigial charge-4e phase. We note that similar 2D and 1D models for triplet superconductors [34–36] and spinor condensates [22] have been previously studied and shown to support charge-4e order.

III. LOCAL SUPPRESSION OF THE COMPETING VESTIGIAL PHASES

A. Formalism for the vestigial orders

Despite being illuminating, the simple model above is not representative of realistic multicomponent superconductors, where either SOC is not negligible or singlet states are realized. Yet, it highlights an efficient strategy to realize charge-4e order: suppression of the other, leading, vestigial phases. While this generally cannot be accomplished globally via Mermin-Wagner's theorem, vestigial nematic or ferromagnetic states tend to form domains to minimize the elastic or magnetic dipolar energies. To explore this idea, we consider a generic two-component superconducting order parameter $\boldsymbol{\Delta} = (\Delta_1, \Delta_2)$, which could describe (p_x, p_y)-wave or (d_{xz}, d_{yz})-wave states in tetragonal and hexagonal lattices [37,38], or $(d_{x^2-y^2}, d_{xy})$-wave pairing in hexagonal systems and 45°-twisted bilayer tetragonal d-wave superconductors [62]. In contrast to the previous example, $\boldsymbol{\Delta}$ now transforms as a two-dimensional IR of a discrete point group. While we will focus on tetragonal (D_{4h}) superconductors, where $\boldsymbol{\Delta}$ transforms as the IR E_g or E_u, the conclusions apply to all other cases.

We start by classifying all possible composite order parameters. As shown in Ref. [46], seven different bilinear combinations can be formed. Apart from the symmetry-preserving bilinear $\Psi^{A_{1g}} = \boldsymbol{\Delta}^\dagger \tau^0 \boldsymbol{\Delta}$, with Pauli matrices τ^i acting on the $\boldsymbol{\Delta}$ subspace, there are three additional real-valued bilinears:

$$\Psi^{A_{2g}} = \boldsymbol{\Delta}^\dagger \tau^y \boldsymbol{\Delta}, \quad \Psi^{B_{1g}} = \boldsymbol{\Delta}^\dagger \tau^z \boldsymbol{\Delta}, \quad \Psi^{B_{2g}} = \boldsymbol{\Delta}^\dagger \tau^x \boldsymbol{\Delta}. \tag{6}$$

Here, $\Psi^{A_{2g}}$ breaks time reversal symmetry and causes ferromagnetism, while $\Psi^{B_{1g}}$ and $\Psi^{B_{2g}}$ break tetragonal symmetry and cause nematicity. The three complex-valued bilinears are given by

$$\psi^{A_{1g}} = \boldsymbol{\Delta}^T \tau^0 \boldsymbol{\Delta}, \quad \psi^{B_{1g}} = \boldsymbol{\Delta}^T \tau^z \boldsymbol{\Delta}, \quad \psi^{B_{2g}} = \boldsymbol{\Delta}^T \tau^x \boldsymbol{\Delta}, \tag{7}$$

and describe, respectively, s-wave, $d_{x^2-y^2}$-wave, and d_{xy}-wave charge-4e superconductivity. In our notation, Ψ^n (ψ^n) denotes real-valued (complex-valued) bilinears, whereas the superscript n indicates the IR according to which the composite transforms. The superconducting action is

$$\mathcal{S} = \int_{\mathsf{x}} r_0 |\boldsymbol{\Delta}_{\mathsf{x}}|^2 + \mathcal{S}^{\text{grad}} + \mathcal{S}^{\text{int}}, \tag{8}$$

where $r_0 = a_0(T - T_0)$ denotes the reference temperature ($a_0, T_0 > 0$) and $\mathcal{S}^{\text{grad}}$ contains the symmetry-allowed gradient terms [38]. The interaction part is given by [46]

$$\mathcal{S}^{\text{int}} = \int_{\mathsf{x}} \left[u \left(\Psi_{\mathsf{x}}^{A_{1g}}\right)^2 + v \left(\Psi_{\mathsf{x}}^{A_{2g}}\right)^2 + w \left(\Psi_{\mathsf{x}}^{B_{1g}}\right)^2\right], \tag{9}$$

and contains three independent interaction parameters $u > 0$ and $v, w > -u$. The mean-field phase diagram in the $(\frac{v}{u}, \frac{w}{u})$ parameter space is well established, displaying chiral and two types of nematic superconductivity [11,38,49].

The vestigial orders associated with each mean-field ground state were analyzed in Ref. [46] via a variational approach. The leading vestigial instability is always that of a real-valued composite (nematic or ferromagnetic), whereas the vestigial charge-4e orders are always subleading. While our conclusions hold across the entire phase diagram, hereafter we focus on the $v > 0 > w$ region [Fig. 1(b)], where the superconducting ground state is nematic and the competing vestigial phases are $d_{x^2-y^2}$-wave nematic ($\Psi^{B_{1g}}$) and s-wave charge-4e ($\psi^{A_{1g}}$). In bulk, the only vestigial order realized is the nematic one [46]. However, because the effective interaction in the charge-4e channel is attractive, the system could gain energy by condensing this mode in regions where nematic order is suppressed. Due to its Ising-like character, $\Psi^{B_{1g}}$ can sustain long-range order at nonzero temperatures. However, because of the linear coupling between $\Psi^{B_{1g}}$ and strain, nematic domains must form to minimize the elastic energy and accommodate long-range lattice deformations. This opens up the possibility of $\psi^{A_{1g}}$ condensation at nematic domain walls.

B. Charge-4e condensation at the domain wall

To proceed, we employ a real-space Gaussian variational approach, which treats all vestigial channels equally, on a 1D grid of length L and $i = 1, \ldots, N$ sites. The variational ansatz consists of a trial action $\mathcal{S}_0$ [46,63–65], which in our case is

$$\mathcal{S}_0 = \frac{1}{2}\frac{L}{T}\sum_i \hat{\boldsymbol{\Delta}}_i^\dagger G_i^{-1} \hat{\boldsymbol{\Delta}}_i + \mathcal{S}^{\text{grad}}, \tag{10}$$

with the gradient contribution $\mathcal{S}^{\text{grad}}$ explicitly given in Eq. (A4). Represented in the Nambu basis $\hat{\boldsymbol{\Delta}}_i = (\boldsymbol{\Delta}_i, \bar{\boldsymbol{\Delta}}_i)$, the local inverse Green's function,

$$G_i^{-1} = \begin{pmatrix} R_i + \Phi_i^{B_{1g}} & \Phi_i^{B_{2g}} - \mathrm{i}\Phi_i^{A_{2g}} & \phi_i^{A_{1g}} + \phi_i^{B_{1g}} & \phi_i^{B_{2g}} \\ & R_i - \Phi_i^{B_{1g}} & \phi_i^{B_{2g}} & \phi_i^{A_{1g}} - \phi_i^{B_{1g}} \\ & & R_i + \Phi_i^{B_{1g}} & \Phi_i^{B_{2g}} + \mathrm{i}\Phi_i^{A_{2g}} \\ \text{H.c.} & & & R_i - \Phi_i^{B_{1g}} \end{pmatrix}, \tag{11}$$

contains the real-valued (Φ_i^n) and complex-valued ($\phi_i^n, \bar{\phi}_i^n$) variational parameters, and the mass renormalization parameter $R_i = r_0 + \Phi_i^{A_{1g}}$. Because $\mathcal{S}_0$ (10) is Gaussian, it is straightforward to compute the variational free energy

$$F_v = -T \log Z_0 + T \langle \mathcal{S} - \mathcal{S}_0 \rangle_0, \tag{12}$$

where $Z_0 = \int D(\mathbf{\Delta}, \bar{\mathbf{\Delta}})\, e^{-\mathcal{S}_0}$ is the partition function of the trial action. The detailed evaluation of Eq. (12) is shown in Appendix A, with the result given in Eq. (A9). Importantly, the original Landau coefficients u, v, and w appear in F_v as different combinations in each symmetry channel, corresponding to effective interactions [46]:

$$\begin{aligned} U_{A_{1g}} &= 3u + v + w, & u_{A_{1g}} &= u - v + w,\\ U_{A_{2g}} &= u + 3v - w, & & \\ U_{B_{1g}} &= u - v + 3w, & u_{B_{1g}} &= u + v + w,\\ U_{B_{2g}} &= u - v - w, & u_{B_{2g}} &= u + v - w. \end{aligned} \tag{13}$$

An attractive interaction ($U_n, u_n < 0$) indicates a potential instability, signaled by the condensation of the corresponding variational order parameter (Φ_i^n, ϕ_i^n). Importantly, a vestigial phase only emerges if superconductivity is not immediately triggered by Φ_i^n, $\phi_i^n \neq 0$. In the variational approach, this condition can be verified by confirming that the variational superconducting susceptibility remains finite. The local superconducting susceptibility χ_i can be derived in the standard way using a conjugate field, see, for example, Ref. [46] for details. Within the phase diagram region of interest ($w < 0 < v$) we find the simple expression

$$\chi_i^{-1} = R_i - \left|\Phi_i^{B_{1g}}\right| - \left|\phi_i^{A_{1g}} - \text{sign}\left(\Phi_i^{B_{1g}}\right)\phi_i^{B_{1g}}\right|. \tag{14}$$

The relationship (14) assumes that all other composite fields are zero, which is also confirmed by our numerics. As is commonly the case [48], the presence of a vestigial order enhances the superconducting susceptibility, and thereby also the transition temperature T_c.

In bulk, for most of the $(\frac{v}{u}, \frac{w}{u})$ phase diagram, there are two competing attractive vestigial-order channels, corresponding to a real-valued composite (nematic/ferromagnetic) and a complex-valued one (s-wave/d-wave charge-$4e$). As demonstrated in Ref. [46], the nematic/ferromagnetic instability is always the leading one in bulk [Fig. 1(b)]. Our goal is to determine the fate of these phases along a nematic domain wall. We therefore numerically minimize the free energy (12) [or Eq. (A9)] for the N-site 1D grid with domain-wall boundary conditions $\Phi_1^{B_{1g}} = -\Phi_N^{B_{1g}} = \Phi_0^{B_{1g}}$, where $\Phi_0^{B_{1g}}$ is the (self-consistently obtained) bulk value of the nematic order parameter (see Appendix B for additional details). Consider first the phase diagram region where the only attractive vestigial-order channel is the nematic, i.e., $U_{B_{1g}} < 0$ but $u_{A_{1g}} > 0$ [red cross in Fig. 1(b)]. The results are shown in Fig. 2. As the control parameter $r_0 \propto T - T_0$ is decreased, a nematic domain emerges below a temperature that coincides with the bulk nematic critical temperature T_{nem}. Note that $T < T_{\text{nem}}$ for all three panels in Fig. 2. As expected, the domain wall becomes sharper as the temperature is lowered, since the wall width scales as $t_0/|\Phi_0^{B_{1g}}|$ where t_0 is the gradient-term stiffness, see Eq. (A4). At the domain-wall center, the superconducting susceptibility χ is suppressed, consistent with the fact that vestigial order enhances the superconducting transition. Interestingly, χ^{-1} has a nonmonotonic spatial dependence, displaying a dip at the domain-wall boundaries, which can lead to local condensation of superconductivity [yellow region of Fig. 2(c)]. No sign of charge-$4e$ order is

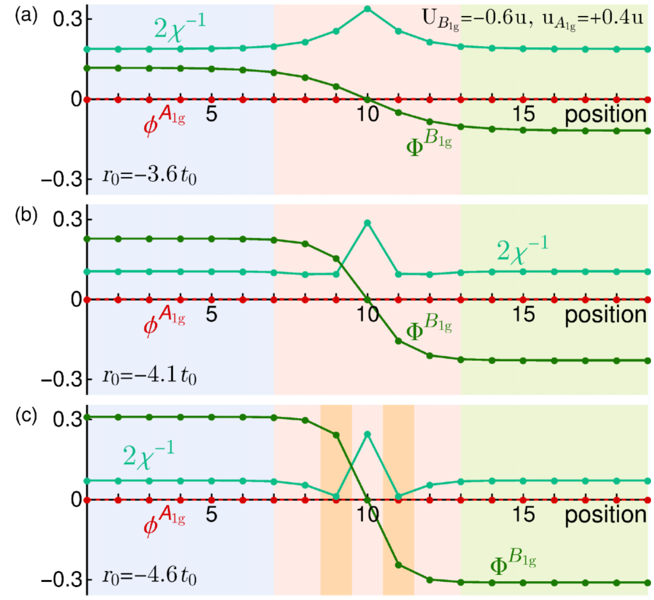

FIG. 2. Variational nematic order parameter ($\Phi^{B_{1g}}$), inverse superconducting susceptibility χ^{-1} (14), and variational charge-$4e$ order parameter ($\phi^{A_{1g}}$) obtained from the numerical minimization of the variational free energy (12) [or Eq. (A9)] across two nematic domains (all in units of the gradient-term stiffness t_0). Each panel corresponds to a different temperature, parametrized by $r_0 \propto T - T_0$. The parameters used here are $w = -0.5u$ and $v = 0.1u$ [red cross in Fig. 1(b)]. Here and in Fig. 3, we set $t_0/\sqrt{uT_0/L} = 20/7$.

observed, consistent with a repulsive effective interaction in this channel.

Consider now the phase-diagram region where the charge-$4e$ vestigial channel is attractive, but subleading to the nematic, $U_{B_{1g}} < u_{A_{1g}} < 0$ [purple cross in Fig. 1(b)]. As shown in Fig. 3(a), nematic order emerges first, and it establishes a domain wall. Now, however, as we lower the temperature [Figs. 3(b) and 3(c)], the charge-$4e$ order parameter $\phi^{A_{1g}}$ condenses inside the domain wall while the superconducting susceptibility χ remains finite. This is the main result of the paper. Because the domain wall is one dimensional, this should be understood as a local condensation, since phase slips will destroy long-range order along the wall. Note, even though the d-wave charge-$4e$ channel is repulsive in this phase-diagram region, the order parameter $\phi^{B_{1g}}$ condenses due to the trilinear coupling between $\Phi^{B_{1g}}$, $\phi^{A_{1g}}$, and $\bar{\phi}^{B_{1g}}$ (see the inset) [46]. We verified that this behavior is not particular to this set of parameters, but occurs in any region of the $(\frac{v}{u}, \frac{w}{u})$ phase diagram where s-wave/d-wave vestigial charge-$4e$ order is sufficiently attractive but subleading to nematic/ferromagnetic vestigial order. The temperature T_{4e}^{local} at which the local condensation occurs can be thought of as the result of a competition between the condensation energy gain and the gradient energy penalty due to the spatially inhomogeneous profile. In this regard, the condensation energy is only available to the system below the temperature T_{4e}^* at which a bulk charge-$4e$ order would occur if it was not suppressed. Correspondingly, local condensation only emerges at $T \lesssim T_{4e}^*$, and it is essential that T_{4e}^* is larger than the SC critical temperature T_c, which can be satisfied for $T_{4e}^* \lesssim T_{\text{nem}}$.

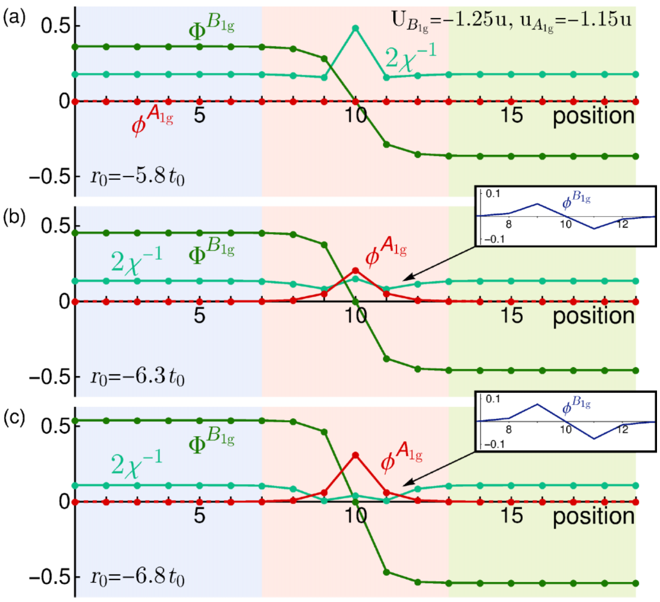

FIG. 3. Same variational parameters as in Fig. 2, but evaluated for the parameters $w = -0.05u$ and $v = 2.1u$ [purple cross in Fig. 1(b)], corresponding to a subleading attractive charge-4e channel ($u_{A_{1g}} < 0$). Local condensation of $\phi^{A_{1g}}$ is observed at the nematic domain wall.

IV. DISCUSSION

In this work, we employed a variational approach to demonstrate that charge-4e order locally condenses at nematic domain walls that emerge in the normal state of nematic superconductors upon approaching the superconducting transition. Before the onset of superconductivity, the system is unstable toward the formation of vestigial nematic and charge-4e orders arising from the fluctuation-induced condensation of composite superconducting order parameters. Because nematic order generally wins over charge-4e order, the suppression of nematic order along the domain wall enables the system to further minimize the free energy by condensing charge-4e order. Since an analogous mechanism also applies for chiral superconductors, our results point to a wide class of systems—multicomponent superconductors—where local charge-4e order can potentially emerge. Among the materials for which there is strong experimental evidence for nematic superconductivity, doped Bi_2Se_3 [43–45,66] and twisted bilayer graphene (TBG) [42,67,68] are the most promising candidates to display this effect. Indeed, a vestigial nematic phase exists in doped Bi_2Se_3 [69,70], whereas in TBG, normal-state nematic order appears close to the superconducting dome [42]. There are also several chiral-superconductor candidates [71], including the widely studied heavy-fermion UPt_3 [39–41].

An important question is how to experimentally detect this effect. Since charge-4e order emerges at nematic domain walls, local probes such as scanning tunneling microscopy (STM) and scanning near-field optical microscopy (SNOM) are ideal. Because the charge-4e state is expected to be gapless [14,15], its density-of-states (DOS) profile, which can be accessed in a standard STM measurement, will likely differ from the normal-state DOS only in subtle ways. On the other hand, Josephson-STM, in which a superconducting tip is used [72,73], could provide more direct evidence for quartets. The SNOM technique has the unique capability of probing the local optical response with a few nanometers resolution, from which the properties of the local optical conductivity $\sigma(\omega, \boldsymbol{r})$ can be inferred [74,75]. Because the charge-4e state has a nonzero superfluid density [15], $\mathrm{Im}\,\sigma(\omega, \boldsymbol{r}) \sim 1/\omega$ is expected to emerge at low frequencies near nematic domain walls. While this behavior could also be due to a charge-2e superconducting filament, only in the charge-4e case this behavior would be accompanied by a gapless DOS, which can be probed via STM. These results also reveal the tantalizing possibility of using uniaxial strain to control the charge-4e phase, since beyond a critical strain value, the sample becomes mononematic domain and local charge-4e order disappears.

ACKNOWLEDGMENTS

We thank J. Schmalian, L. Fu, and R. Willa for fruitful discussions, and particularly Y. Wang for in-depth discussions about the properties of charge-4e superconductors. This work was supported by the U.S. Department of Energy, Office of Science, Basic Energy Sciences, Materials Sciences and Engineering Division, under Award No. DE-SC0020045.

APPENDIX A: DERIVATION OF THE VARIATIONAL FREE ENERGY

Here, we derive the variational free energy associated with the ansatz $\mathcal{S}_0$, i.e., we evaluate Eq. (12). For convenience, we first repeat the setup of the problem and the notations introduced in the main text. Expressing the two-component superconducting order parameter $\boldsymbol{\Delta} = (\Delta_1, \Delta_2)$ in terms of the four-component Nambu basis $\hat{\boldsymbol{\Delta}} = (\boldsymbol{\Delta}, \bar{\boldsymbol{\Delta}})$, we can rewrite the real-valued and complex-valued bilinear combinations as

$$\Psi^n = \hat{\boldsymbol{\Delta}}^\dagger M^n \hat{\boldsymbol{\Delta}}, \quad \psi^n = \hat{\boldsymbol{\Delta}}^\dagger m^n \hat{\boldsymbol{\Delta}}. \tag{A1}$$

Here, we defined the matrices

$$\begin{aligned} M^{A_{1g}} &= \tau^0\sigma^0/2, \quad m^{A_{1g}} = \tau^0\sigma^-, \quad M^{A_{2g}} = \tau^y\sigma^z/2,\\ M^{B_{1g}} &= \tau^z\sigma^0/2, \quad m^{B_{1g}} = \tau^z\sigma^-,\\ M^{B_{2g}} &= \tau^x\sigma^0/2, \quad m^{B_{2g}} = \tau^x\sigma^- \end{aligned} \tag{A2}$$

with $\sigma^\pm = (\sigma^x \pm i\sigma^y)/2$ and τ^i, σ^i acting respectively on the internal superconducting subspace and on the Nambu space. For our specific setting of a one-dimensional grid of length L with lattice sites labeled $i, j = 1, \dots, N$, the superconducting action becomes

$$\mathcal{S} = \frac{L}{T}\sum_{i,j} \boldsymbol{\Delta}_i^\dagger \left[r_0\delta_{ij} + \frac{1}{2}f_{ij}^0\right]\tau^0\boldsymbol{\Delta}_j \;+\; \mathcal{S}^{\mathrm{int}}, \tag{A3}$$

where we introduced the gradient term

$$\mathcal{S}^{\mathrm{grad}} = \frac{L}{2T}\sum_{i,j} \boldsymbol{\Delta}_i^\dagger \tau^0 f_{ij}^0 \boldsymbol{\Delta}_j, \tag{A4}$$

described in terms of the hopping function $f_{ij}^0 = \frac{t_0}{2}(2\delta_{ij} - \delta_{i,j+1} - \delta_{i,j-1})$ and the stiffness parameter $t_0 > 0$. Recall that $r_0 = a_0(T - T_0)$ denotes the bare superconducting transition temperature with $a_0, T_0 > 0$. The interaction part is given by [46] [see also Eq. (9)]

$$\mathcal{S}^{\text{int}} = \frac{L}{T}\sum_i \left[u\left(\Psi_i^{A_{1g}}\right)^2 + v\left(\Psi_i^{A_{2g}}\right)^2 + w\left(\Psi_i^{B_{1g}}\right)^2\right], \tag{A5}$$

where the Landau parameters satisfy the conditions $u > 0$ and $v, w > -u$ in order for the action to be bounded.

As discussed in the main text, within the Gaussian variational approach, we choose a trial action [cf. also Eq. (10)],

$$\mathcal{S}_0 = \frac{1}{2}\frac{L}{T}\sum_{i,j} \hat{\mathbf{\Delta}}_i^\dagger \, \mathcal{G}_{i,j}^{-1} \, \hat{\mathbf{\Delta}}_j, \tag{A6}$$

that is characterized by the inverse Green's function

$$\mathcal{G}_{ij}^{-1} = G_i^{-1}\,\delta_{ij} + f_{ij}^0 M^{A_{1g}}, \tag{A7}$$

$$G_i^{-1} = 2R_i M^{A_{1g}} + 2\sum_{n\in\mathbb{G}_\mathbb{R}} \Phi_i^n M^n + \sum_{n\in\mathbb{G}_\mathbb{C}} \left(\bar{\phi}_i^n m^n + \text{H.c.}\right), \tag{A8}$$

which contains all variational parameters. Recall that we use Φ_i^n for real-valued variational composite order parameters and $(\phi_i^n, \bar{\phi}_i^n)$ for the complex-valued ones, where n denotes the irreducible representation (IR) according to which the composite transforms. Moreover, we also define the mass renormalization parameter $R_i = r_0 + \Phi_i^{A_{1g}}$. For convenience of notation, we introduce the IR sets $\mathbb{G}_\mathbb{R} = \{A_{2g}, B_{1g}, B_{2g}\}$ and $\mathbb{G}_\mathbb{C} = \{A_{1g}, B_{1g}, B_{2g}\}$ in Eq. (A8). Note that the local inverse Green's function (A8) is identical to Eq. (11).

Since the trial action (A6) is Gaussian, it is straightforward to evaluate the variational free energy F_v, Eq. (12), see, for example, Ref. [46] for technical details. In the real-space representation (A6) it is convenient to promote the 4-component field $\hat{\mathbf{\Delta}}_i$ to a $(4N)$-component field via $\hat{\hat{\mathbf{\Delta}}} = \sum_i \hat{P}_i \hat{\mathbf{\Delta}}_i$, where the projector $\hat{P}_i$ is a $(4N) \times 4$ dimensional matrix whose elements are either zero or one, and $\hat{P}_i^T \hat{P}_j = \delta_{ij}\mathbb{1}_4$. The resulting variational free energy F_v, up to an unimportant constant, is given by

$$F_v = \frac{T}{2}\log\det(\hat{\hat{\mathcal{G}}}^{-1}) + T\sum_i \Big\{ 2\big[r_0 - R_i + \tilde{U}_{A_{1g}} G_{ii}^{A_{1g}}\big] G_{ii}^{A_{1g}} - 2\sum_{n\in\mathbb{G}_\mathbb{R}} \left(\Phi_i^n - \tilde{U}_n G_{ii}^n\right) G_{ii}^n - \sum_{n\in\mathbb{G}_\mathbb{C}} \left[\left(\phi_i^n - \tilde{u}_n g_{ii}^n\right)\bar{g}_{ii}^n + \text{c.c.}\right]\Big\}. \tag{A9}$$

Here, $\hat{\hat{\mathcal{G}}}$ is the inverse of $\hat{\hat{\mathcal{G}}}^{-1} = \sum_{i,j} \hat{P}_i \mathcal{G}_{ij}^{-1} \hat{P}_j^T$ and G_{ij}^n is given by the decomposition of $\mathcal{G}_{ij} = \hat{P}_i^T \hat{\hat{\mathcal{G}}} \hat{P}_j$ onto the symmetry channels according to

$$\mathcal{G}_{ij} = 2\sum_{n\in\{A_{1g},\mathbb{G}_\mathbb{R}\}} G_{ij}^n M^n + \sum_{n\in\mathbb{G}_\mathbb{C}} \left[g_{ij}^n (m^n)^\dagger + \bar{g}_{ij}^n m^n\right]. \tag{A10}$$

Finally, in Eq. (A9), the effective interaction parameters $\{\tilde{U}_n, \tilde{u}_n\} = \frac{T}{L}\{U_n, u_n\}$ in each symmetry channel are given by Eq. (13), which agrees with the expressions found in the bulk case [46].

APPENDIX B: DETAILS OF THE FREE ENERGY MINIMIZATION

In this section, we present a few technical details related to the minimization of the variational free energy (A9). The implemented Matlab code can be found in Ref. [76]. As emphasized in the main text, we model the domain wall through the boundary conditions $\Phi_1^{B_{1g}} = -\Phi_N^{B_{1g}} = \Phi_0^{B_{1g}}$, $R_1 = R_N = R_0$, and all other fields $\Phi_{1,N}^n = \phi_{1,N}^n = 0$, where $\Phi_0^{B_{1g}}$ and R_0 are the corresponding bulk values.

The free energy (A9) effectively depends only on the parameters T, $\hat{t}_0 \equiv t_0/\sqrt{uT/L}$, $\{v, w\}/u$, and $\{r_0, R_i, \Phi_i^n, \phi_i^n\}/t_0$. In the spirit of the Ginzburg-Landau approach, we assume the most important temperature dependence to be in $r_0 = a_0(T - T_0)$, and we set $T = T_0$ elsewhere, with T_0 denoting the SC reference temperature. To facilitate the minimization of the free energy (A9), we supply the minimizer with the gradient expressions given by

$$\frac{\partial F_v}{\partial X_i} = T\sum_j \left\{ V_j^{A_{1g}} \frac{\partial G_{jj}^{A_{1g}}}{\partial X_i} + \sum_{n\in\mathbb{G}_\mathbb{R}} V_j^n \frac{\partial G_{jj}^n}{\partial X_i} + \sum_{n\in\mathbb{G}_\mathbb{C}} \left(v_j^n \frac{\partial g_{jj}^n}{\partial X_i} + \text{c.c.}\right)\right\}, \tag{B1}$$

where $X_i \in \{R_i, \Phi_i^n, \phi_i^n, \bar{\phi}_i^n\}$ can be any of the variational parameters. In writing Eq. (B1), we exploited the fact that the partial derivatives $\frac{\partial F_v}{\partial X_i}|_{G^n,g^n} = 0$ vanish [46]. Moreover, we defined

$$V_j^{A_{1g}} = 2\big[r_0 - R_j + 2\tilde{U}_{A_{1g}} G_{jj}^{A_{1g}}\big], \quad v_j^n = -\left(\bar{\phi}_j^n - 2\tilde{u}_n \bar{g}_{jj}^n\right),$$
$$V_j^n = -2\left(\Phi_j^n - 2\tilde{U}_n G_{jj}^n\right). \tag{B2}$$

To determine the remaining derivatives in Eq. (B1), we use the Green's function (A10) to identify

$$G_{jj}^n = \frac{1}{2}\text{tr}[\mathcal{G}_{jj} M^n], \quad g_{jj}^n = \frac{1}{2}\text{tr}[\mathcal{G}_{jj} m^n]. \tag{B3}$$

Then, using the introduced projector matrix $\hat{P}_i$, we obtain the relationship

$$\frac{\partial \mathcal{G}_{jj}}{\partial X_i} = -\hat{P}_j^T \hat{\hat{\mathcal{G}}} \frac{\partial \hat{\hat{\mathcal{G}}}^{-1}}{\partial X_i} \hat{\hat{\mathcal{G}}} \hat{P}_j = -\sum_{i_1 i_2} \mathcal{G}_{j i_1} \frac{\partial \mathcal{G}_{i_1 i_2}^{-1}}{\partial X_i} \mathcal{G}_{i_2 j}, \tag{B4}$$

which leads to the expressions

$$\frac{\partial \mathcal{G}_{jj}}{\partial R_i} = -2\mathcal{G}_{ji} M^{A_{1g}} \mathcal{G}_{ij}, \quad \frac{\partial \mathcal{G}_{jj}}{\partial \Phi_i^n} = -2\mathcal{G}_{ji} M^n \mathcal{G}_{ij},$$
$$\frac{\partial \mathcal{G}_{jj}}{\partial \bar{\phi}_i^n} = -\mathcal{G}_{ji} m^n \mathcal{G}_{ij}. \tag{B5}$$

It is now straightforward to compute the derivatives in Eq. (B1) by using Eqs. (B5) and (B3); we find, for instance,

$$\frac{\partial G_{jj}^n}{\partial R_i} = -\text{tr}[\mathcal{G}_{ji} M^{A_{1g}} \mathcal{G}_{ij} M^n],$$
$$\frac{\partial g_{jj}^n}{\partial R_i} = -\text{tr}[\mathcal{G}_{ji} M^{A_{1g}} \mathcal{G}_{ij} m^n], \tag{B6}$$

and similar expressions for the other variational parameters.

[1] J. Valatin and D. Butler, On the collective properties of a boson system, Nuovo Cim. **10**, 37 (1958).
[2] W. Evans and Y. Imry, On the pairing theory of the bose superfluid, Nuov. Cim. B **63**, 155 (1969).
[3] G. Röpke, A. Schnell, P. Schuck, and P. Nozières, Four-particle condensate in strongly coupled Fermion systems, Phys. Rev. Lett. **80**, 3177 (1998).
[4] M. A. Lampert, Mobile and immobile effective-mass-particle complexes in nonmetallic solids, Phys. Rev. Lett. **1**, 450 (1958).
[5] S. A. Moskalenko, The theory of Mott exciton in alkali-halide crystals, Opt. Spektrosk **5**, 147 (1958).
[6] Z. Wang, A. E. Feiguin, W. Zhu, O. A. Starykh, A. V. Chubukov, and C. D. Batista, Chiral liquid phase of simple quantum magnets, Phys. Rev. B **96**, 184409 (2017).
[7] J. Strockoz, D. S. Antonenko, D. LaBelle, and J. W. Venderbos, Excitonic instability towards a Potts-nematic quantum paramagnet, Phys. Rev. Res. **6**, 023034 (2024).
[8] S. E. Korshunov, Two-dimensional superfluid Fermi liquid with *p*-pairing, Zh. Eksp. Teor. Fiz. **89**, 539 (1985).
[9] G. E. Volovik, *Exotic Properties of Superfluid* ^{3}He, Series in Modern Condensed Matter Physics, Vol. 1 (World Scientific, 1992).
[10] A. A. Aligia, A. P. Kampf, and J. Mannhart, Quartet formation at (100)/(110) interfaces of *d*-wave superconductors, Phys. Rev. Lett. **94**, 247004 (2005).
[11] E. Berg, E. Fradkin, and S. A. Kivelson, Charge-4*e* superconductivity from pair-density-wave order in certain high-temperature superconductors, Nat. Phys. **5**, 830 (2009).
[12] E.-G. Moon, Skyrmions with quadratic band touching fermions: A way to achieve charge 4*e* superconductivity, Phys. Rev. B **85**, 245123 (2012).
[13] E. Khalaf, P. Ledwith, and A. Vishwanath, Symmetry constraints on superconductivity in twisted bilayer graphene: Fractional vortices, 4*e* condensates, or nonunitary pairing, Phys. Rev. B **105**, 224508 (2022).
[14] Y.-F. Jiang, Z.-X. Li, S. A. Kivelson, and H. Yao, Charge-4*e* superconductors: A Majorana quantum Monte Carlo study, Phys. Rev. B **95**, 241103(R) (2017).
[15] N. V. Gnezdilov and Y. Wang, Solvable model for a charge-4*e* superconductor, Phys. Rev. B **106**, 094508 (2022).
[16] J. Ge, P. Wang, Y. Xing, Q. Yin, H. Lei, Z. Wang, and J. Wang, Evidence for multi-charge flux quantization in kagome superconductor ring devices, arXiv:2201.10352.
[17] C. M. Varma and Z. Wang, Extended superconducting fluctuation region and 6*e* and 4*e* flux quantization in a kagome compound with a normal state of 3*Q* order, Phys. Rev. B **108**, 214516 (2023).
[18] P. Noziéres and D. Saint James, Particle vs. pair condensation in attractive Bose liquids, J. de Phys. **43**, 1133 (1982).
[19] A. B. Kuklov and B. V. Svistunov, Counterflow superfluidity of two-species ultracold atoms in a commensurate optical lattice, Phys. Rev. Lett. **90**, 100401 (2003).
[20] E. Babaev, A. Sudbø, and N. Ashcroft, A superconductor to superfluid phase transition in liquid metallic hydrogen, Nature (London) **431**, 666 (2004).
[21] C. Wu, Competing orders in one-dimensional spin-3/2 fermionic systems, Phys. Rev. Lett. **95**, 266404 (2005).
[22] S. Mukerjee, C. Xu, and J. E. Moore, Topological defects and the superfluid transition of the $s = 1$ spinor condensate in two dimensions, Phys. Rev. Lett. **97**, 120406 (2006).
[23] E. V. Herland, E. Babaev, and A. Sudbø, Phase transitions in a three dimensional $U(1) \times U(1)$ lattice London superconductor: Metallic superfluid and charge-4*e* superconducting states, Phys. Rev. B **82**, 134511 (2010).
[24] L. Radzihovsky and A. Vishwanath, Quantum liquid crystals in an imbalanced Fermi gas: Fluctuations and fractional vortices in Larkin-Ovchinnikov states, Phys. Rev. Lett. **103**, 010404 (2009).
[25] L. Radzihovsky, Fluctuations and phase transitions in Larkin-Ovchinnikov liquid-crystal states of a population-imbalanced resonant Fermi gas, Phys. Rev. A **84**, 023611 (2011).
[26] D. F. Agterberg, M. Geracie, and H. Tsunetsugu, Conventional and charge-six superfluids from melting hexagonal Fulde-Ferrell-Larkin-Ovchinnikov phases in two dimensions, Phys. Rev. B **84**, 014513 (2011).
[27] D. F. Agterberg, J. C. S. Davis, S. D. Edkins, E. Fradkin, D. J. V. Harlingen, S. A. Kivelson, P. A. Lee, L. Radzihovsky, J. M. Tranquada, and Y. Wang, The physics of pair-density waves: Cuprate superconductors and beyond, Annu. Rev. Condens. Matter Phys. **11**, 231 (2020).
[28] D. Shaffer, F. J. Burnell, and R. M. Fernandes, Weak-coupling theory of pair density wave instabilities in transition metal dichalcogenides, Phys. Rev. B **107**, 224516 (2023).
[29] Y. Yu, Nondegenerate surface pair density wave in the kagome superconductor CsV_3Sb_5: Application to vestigial orders, Phys. Rev. B **108**, 054517 (2023).
[30] Y.-M. Wu and Y. Wang, *d*-wave charge-4*e* superconductivity from fluctuating pair density waves, arXiv:2303.17631.
[31] R. M. Fernandes and L. Fu, Charge-4*e* superconductivity from multicomponent nematic pairing: Application to twisted bilayer graphene, Phys. Rev. Lett. **127**, 047001 (2021).
[32] S.-K. Jian, Y. Huang, and H. Yao, Charge-4*e* superconductivity from nematic superconductors in two and three dimensions, Phys. Rev. Lett. **127**, 227001 (2021).
[33] M. Zeng, L.-H. Hu, H.-Y. Hu, Y.-Z. You, and C. Wu, High-order time-reversal symmetry breaking normal state, Sci. China Phys. Mech. Astron. **67**, 237411 (2024).
[34] M. A. Rampp, E. J. König, and J. Schmalian, Topologically enabled superconductivity, Phys. Rev. Lett. **129**, 077001 (2022).
[35] J. B. Curtis, N. R. Poniatowski, Y. Xie, A. Yacoby, E. Demler, and P. Narang, Stabilizing fluctuating spin-triplet superconductivity in graphene via induced spin-orbit coupling, Phys. Rev. Lett. **130**, 196001 (2023).
[36] P. P. Poduval and M. S. Scheurer, Vestigial singlet pairing in a fluctuating magnetic triplet superconductor: Applications to graphene moiré systems, Nat. Commun. **15**, 1713 (2024).
[37] J. F. Annett, Symmetry of the order parameter for high-temperature superconductivity, Adv. Phys. **39**, 83 (1990).
[38] M. Sigrist and K. Ueda, Phenomenological theory of unconventional superconductivity, Rev. Mod. Phys. **63**, 239 (1991).
[39] J. Sauls, The order parameter for the superconducting phases of UPt_3, Adv. Phys. **43**, 113 (1994).
[40] E. Schemm, W. Gannon, C. Wishne, W. Halperin, and A. Kapitulnik, Observation of broken time-reversal symmetry in the heavy-fermion superconductor UPt_3, Science **345**, 190 (2014).
[41] K. E. Avers, W. J. Gannon, S. J. Kuhn, W. P. Halperin, J. Sauls, L. DeBeer-Schmitt, C. Dewhurst, J. Gavilano, G. Nagy, U. Gasser *et al.*, Broken time-reversal symmetry in the topological superconductor UPt_3, Nat. Phys. **16**, 531 (2020).

[42] Y. Cao, D. Rodan-Legrain, J. M. Park, N. F. Yuan, K. Watanabe, T. Taniguchi, R. M. Fernandes, L. Fu, and P. Jarillo-Herrero, Nematicity and competing orders in superconducting magic-angle graphene, Science **372**, 264 (2021).

[43] K. Matano, M. Kriener, K. Segawa, Y. Ando, and G.-Q. Zheng, Spin-rotation symmetry breaking in the superconducting state of $Cu_xBi_2Se_3$, Nat. Phys. **12**, 852 (2016).

[44] Y. Pan, A. Nikitin, G. Araizi, Y. Huang, Y. Matsushita, T. Naka, and A. De Visser, Rotational symmetry breaking in the topological superconductor $Sr_xBi_2Se_3$ probed by upper-critical field experiments, Sci. Rep. **6**, 28632 (2016).

[45] T. Asaba, B. J. Lawson, C. Tinsman, L. Chen, P. Corbae, G. Li, Y. Qiu, Y. S. Hor, L. Fu, and L. Li, Rotational symmetry breaking in a trigonal superconductor *Nb*-doped Bi_2Se_3, Phys. Rev. X **7**, 011009 (2017).

[46] M. Hecker, R. Willa, J. Schmalian, and R. M. Fernandes, Cascade of vestigial orders in two-component superconductors: Nematic, ferromagnetic, *s*-wave charge-4*e*, and *d*-wave charge-4*e* states, Phys. Rev. B **107**, 224503 (2023).

[47] E. Fradkin, S. A. Kivelson, and J. M. Tranquada, Colloquium: Theory of intertwined orders in high temperature superconductors, Rev. Mod. Phys. **87**, 457 (2015).

[48] R. M. Fernandes, P. P. Orth, and J. Schmalian, Intertwined vestigial order in quantum materials: Nematicity and beyond, Annu. Rev. Condens. Matter Phys. **10**, 133 (2019).

[49] V. Gali and R. M. Fernandes, Role of electromagnetic gauge-field fluctuations in the selection between chiral and nematic superconductivity, Phys. Rev. B **106**, 094509 (2022).

[50] M. Hecker and J. Schmalian, Vestigial nematic order and superconductivity in the doped topological insulator $Cu_xBi_2Se_3$, npj Quantum Mater. **3**, 26 (2018).

[51] R. Willa, Symmetry-mixed bound-state order, Phys. Rev. B **102**, 180503(R) (2020).

[52] B. Leridon, S. Caprara, J. Vanacken, V. V. Moshchalkov, B. Vignolle, R. Porwal, R. C. Budhani, A. Attanasi, M. Grilli, and J. Lorenzana, Protected superconductivity at the boundaries of charge-density-wave domains, New J. Phys. **22**, 073025 (2020).

[53] J. W. F. Venderbos and R. M. Fernandes, Correlations and electronic order in a two-orbital honeycomb lattice model for twisted bilayer graphene, Phys. Rev. B **98**, 245103 (2018).

[54] M. S. Scheurer and R. Samajdar, Pairing in graphene-based moiré superlattices, Phys. Rev. Res. **2**, 033062 (2020).

[55] Y. Wang, J. Kang, and R. M. Fernandes, Topological and nematic superconductivity mediated by ferro-su(4) fluctuations in twisted bilayer graphene, Phys. Rev. B **103**, 024506 (2021).

[56] E. Lake, A. S. Patri, and T. Senthil, Pairing symmetry of twisted bilayer graphene: A phenomenological synthesis, Phys. Rev. B **106**, 104506 (2022).

[57] Z. Dong, A. V. Chubukov, and L. Levitov, Transformer spin-triplet superconductivity at the onset of isospin order in bilayer graphene, Phys. Rev. B **107**, 174512 (2023).

[58] G. E. Volovik and L. P. Gor'kov, Superconducting classes in heavy-fermion systems, Zh. Eksp. Teor. Fiz. **88**, 1412 (1985).

[59] E. J. Blagoeva, G. Busiello, L. De Cesare, Y. T. Millev, I. Rabuffo, and D. I. Uzunov, Fluctuation-induced first-order transitions in unconventional superconductors, Phys. Rev. B **42**, 6124 (1990).

[60] M. Blume and Y. Hsieh, Biquadratic exchange and quadrupolar ordering, J. Appl. Phys. **40**, 1249 (1969).

[61] A. F. Andreev and I. A. Grishchuk, Spin nematics, Sov. Phys. JETP **60**, 267 (1984).

[62] R. Haenel, T. Tummuru, and M. Franz, Incoherent tunneling and topological superconductivity in twisted cuprate bilayers, Phys. Rev. B **106**, 104505 (2022).

[63] M. Moshe and J. Zinn-Justin, Quantum field theory in the large N limit: A review, Phys. Rep. **385**, 69 (2003).

[64] M. H. Fischer and E. Berg, Fluctuation and strain effects in a chiral *p*-wave superconductor, Phys. Rev. B **93**, 054501 (2016).

[65] L. Nie, A. V. Maharaj, E. Fradkin, and S. A. Kivelson, Vestigial nematicity from spin and/or charge order in the cuprates, Phys. Rev. B **96**, 085142 (2017).

[66] L. Fu, Odd-parity topological superconductor with nematic order: Application to $Cu_xBi_2Se_3$, Phys. Rev. B **90**, 100509(R) (2014).

[67] V. Kozii, H. Isobe, J. W. F. Venderbos, and L. Fu, Nematic superconductivity stabilized by density wave fluctuations: Possible application to twisted bilayer graphene, Phys. Rev. B **99**, 144507 (2019).

[68] D. V. Chichinadze, L. Classen, and A. V. Chubukov, Nematic superconductivity in twisted bilayer graphene, Phys. Rev. B **101**, 224513 (2020).

[69] Y. Sun, S. Kittaka, T. Sakakibara, K. Machida, J. Wang, J. Wen, X. Xing, Z. Shi, and T. Tamegai, Quasiparticle evidence for the nematic state above T_c in $Sr_xBi_2Se_3$, Phys. Rev. Lett. **123**, 027002 (2019).

[70] C.-w. Cho, J. Shen, J. Lyu, O. Atanov, Q. Chen, S. H. Lee, Y. San Hor, D. J. Gawryluk, E. Pomjakushina, M. Bartkowiak, M. Hecker, J. Schmalian, and R. Lortz, Z_3-vestigial nematic order due to superconducting fluctuations in the doped topological insulator $Nb_xBi_2Se_3$ and $Cu_xBi_2Se_3$, Nat. Commun. **11**, 1 (2020).

[71] S. K. Ghosh, M. Smidman, T. Shang, J. F. Annett, A. D. Hillier, J. Quintanilla, and H. Yuan, Recent progress on superconductors with time-reversal symmetry breaking, J. Phys.: Condens. Matter **33**, 033001 (2021).

[72] O. Naaman, W. Teizer, and R. C. Dynes, Fluctuation dominated josephson tunneling with a scanning tunneling microscope, Phys. Rev. Lett. **87**, 097004 (2001).

[73] K. M. Bastiaans, D. Cho, D. Chatzopoulos, M. Leeuwenhoek, C. Koks, and M. P. Allan, Imaging doubled shot noise in a Josephson scanning tunneling microscope, Phys. Rev. B **100**, 104506 (2019).

[74] H. U. Yang, E. Hebestreit, E. E. Josberger, and M. B. Raschke, A cryogenic scattering-type scanning near-field optical microscope, Rev. Sci. Instrum. **84**, 023701 (2013).

[75] A. S. McLeod, E. van Heumen, J. G. Ramirez, S. Wang, T. Saerbeck, S. Guenon, M. Goldflam, L. Anderegg, P. Kelly, A. Mueller, M. K. Liu, I. K. Schuller, and D. N. Basov, Nanotextured phase coexistence in the correlated insulator V_2O_3, Nat. Phys. **13**, 80 (2017).

[76] M. Hecker, Local charge-4*e* condensation (Matlab code) (2024), https://github.com/hecker-m/Local_Charge-4e_Condensation.